Contents lists available at ScienceDirect

International Journal of Multiphase Flow

A new model for disturbance waves

N.S. Hall Taylor [a], I.J. Hewitt [a,*], J.R. Ockendon [a], T.P. Witelski [b]

[a] Mathematical Institute, University of Oxford, Radcliffe Observatory Quarter, Woodstock Road, Oxford OX2 6GG, UK
[b] Mathematics Department, Duke University, Box 90320, Durham, NC 27708-0320, USA

A R T I C L E   I N F O

A B S T R A C T

The first part of this paper surveys the distinctive features of trains of disturbance waves in high-speed annular two-phase flow. This data is then used to construct a mathematical model that predicts relations between the speed, height, and spacing of the waves, and the net liquid flow rate. These relations highlight the importance of the vorticity in the waves, a quantity that has received little experimental attention.

1. Introduction

There are several flow regimes in gas liquid two-phase flow, one of the most important of which is annular flow (Hewitt and Hall Taylor, 1970). This is the dominant regime in, for example, conventional and nuclear boilers, refrigeration systems, transfer lines and the extraction of crude oil and natural gas.

In annular flow the gas phase moves in the core of a tube surrounded by a thin liquid film on the tube wall. For most combinations of materials for the gas and liquid phases, in typical flow regimes, the film surface is composed of small ripples and larger waves. Some of these are non-coherent and non-persistent (Belt et al., 2010) but, importantly for heat and mass transfer, there exist states where the interface can take the form of a train of what have become known as 'disturbance waves'. These are large amplitude waves having a regular height much greater than the minimum film thickness, and large regular separations, being two or three orders of magnitude greater than their height.

Disturbance waves are known to cause entrainment of droplets from the liquid to the gas phase, causing the gas phase itself to be a two-phase mixture of gas and entrained droplets. The waves also act as a source of surface roughness acting on the gas flow and so are a determining influence on the pressure gradient. Thus an understanding of the character of disturbance waves is essential when trying to propose phenomenological analyses of annular two-phase flow.

A schematic picture of the development of the waves, introducing some of our notation, is shown in Fig. 1.

In this paper we attempt to provide a basic understanding of these waves, by modelling them mathematically as moving packets of inviscid liquid. In Section 2, we examine some of the experimental data available to determine the generic character of disturbance waves. Then in Section 3 we propose a mathematical model that appears to be consistent with these observations, and in Section 4 we discuss the predictions of the model and their implications.

For the higher liquid and gas flow rates discussed in this paper the effect of inertia dominates over the effect of gravity (see de Jong and Gabriel, 2003 for a more detailed discussion), and we therefore ignore gravity throughout. Also, both the gas and liquid Reynolds numbers, based on the tube radius and film thickness respectively, are so large that the effects of viscosity can largely be ignored, as will be the effects of gas compressibility.

2. Experimental data

When annular flow takes place in a transparent tube, the disturbance waves can be clearly observed by eye as travelling milky bands, the milkiness being due to the light scattering effect occurring at their uneven interface. Early results were obtained by frame-by-frame analysis of cine films (Hall Taylor et al., 1963; Nedderman and Shearer, 1963), but conductance probe methods were soon developed which greatly enhanced the speed of analysis (*e.g.* Wang et al., 2004).

The early data only related to the macroscale characteristics of wave velocity, frequency and separation under different

---

* Corresponding author.
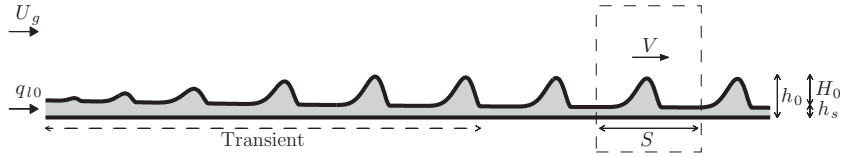 *E-mail address:* hewitt@maths.ox.ac.uk (I.J. Hewitt).

Fig. 1. Schematic of the development of disturbance waves along the wall of a tube (not to scale). The gas speed is U_g, and initial liquid flow rate is q_{l0}. Interfacial waves form on the surface of the film and following an initial entry region they grow towards a uniform train with constant wave speed V and separation S. The film thickness on the tube wall is denoted h; in Section 2 this is partitioned into the uniform sub-layer thickness h_s and wave height $H = h - h_s$. The respective maximum heights are denoted h_0 and H_0. Section 3 will examine the form of the wave in the moving frame shown in the dashed-line box.

combinations of liquid and gas flow. The use of conductance probes and other methods of measurement have become more refined over time and it is now possible to obtain data, with varying levels of detail, of the interface shape and hence values of wave height and minimum thickness. Other methods for obtaining this information use laser focussed displacement meters (LFDM) (Hazuku et al., 2008), planar laser-induced florescence (PLIF) (Schubring et al., 2010, Pt II) and high-speed back-lit video (Schubring et al., 2010, Pt I).

These more detailed studies reveal that the interface structure is very complicated on scales below the disturbance-wave length, but the disturbance waves themselves show remarkably consistent properties when viewed on the macro-scale. Indeed, the actual disturbance waves, once formed, remain axially and circumferentially coherent (Zhao et al., 2013), and the supporting experimental evidence for these phenomena will be presented in the following subsections. Unfortunately, the scenario is inevitably obscured by the small ripples and non-coherent waves which occur on and between the disturbance waves.

2.1. Spatial evolution of disturbance waves

Most of the following observations have been made using the valuable data reported by Wolf et al. (2001) and de Jong and Gabriel (2003). From the work of Wolf et al. it is apparent that interfacial waves form very close to the tube inlet where the gas and liquid phases first intersect. Moving along the tube, there is a transition region where the waves both accelerate and coalesce. During this transition region, the waves become coherent and, as the work of Zhao et al. (2013) shows, the waves become circumferentially coherent (i.e. axisymmetric) beyond a distance of about 20 tube diameters (D); it is only after this distance we can sensibly refer to the interfacial variations as disturbance waves.

As Fig. 2(a,b) shows, the velocity V and separation S of these coherent waves become essentially constant after a length $L \approx 30D$. However, as mentioned in the introduction, interfacial waves often generate droplet entrainment, so that the liquid flow in the film drops off with distance, as shown in Fig. 2(c). This suggests a downward trend towards a constant average film thickness, but over a longer relaxation distance than for V and S. This reflects the fact that the change in film flow is determined by the balance between the rate of entrainment and the rate of deposition of droplets from the gas phase back into the film. For the higher liquid flows the cumulative loss of mass due to entrainment can be as much as 50%. However this reduction takes place over a distance of at least $L/D = 100$, much longer than the $L/D = 30$ needed to reach the constant velocity and constant separation of the waves.

We infer from this that the entrainment of droplets, while important in determining the liquid flow in the film, is not a key mechanism for the establishment and persistence of the disturbance waves. Henceforth, we will be concerned with the behaviour of the disturbance waves at long distances from the inlet.
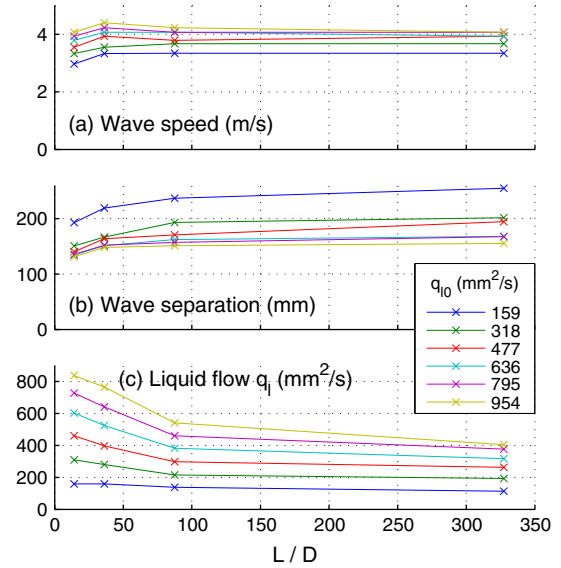

Fig. 2. Change of wave speed, separation, and liquid flow rate, with distance along the tube, for different initial liquid flow rates q_{l0} (mm²/s). The gas velocity U_g is fixed at 34 m/s. (Data from Wolf et al. (2001)).
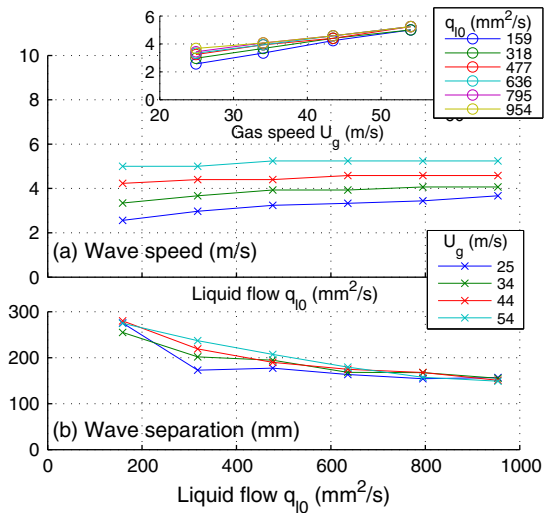

Fig. 3. Wave speed (a) and separation (b) against initial liquid flow, for different gas speed in a 32 mm tube. The inset in (a) shows the same data for wave speed plotted as a function of gas speed, for different initial liquid flows. (Data from Wolf et al. (2001)).

2.2. Dependence on flow rates

We begin by recalling the work of Wolf et al. (2001), who obtained their data in a 31.8 mm tube and took readings at

$L/D = 300$, by which stage a near equilibrium condition has been attained. Fig. 3a indicates that the wave velocity increases weakly with the liquid flow but increases more strongly, and approximately linearly, with the gas velocity, while Fig. 3b shows that the equilibrium separation is essentially independent of the gas velocity. There is a decreasing separation with increasing liquid flow but this also tends to a fairly constant value of about 150 mm at large flow rates, regardless of gas velocity. We also remark that the wave speed is always an order of magnitude less than the gas speed, a fact that will simplify the modelling in Section 3.

It is interesting to compare these results with those of de Jong and Gabriel (2003), who took their readings in a 9.5 mm tube at a distance of $L/D = 110$. Their separation data is given in Fig. 4, which similarly indicates that the separation tends to a constant value independent of both liquid and gas flow rates, as U_g increases. In this case the limiting separation appears to be slightly lower, at about 130 mm.

The literature we have cited reveals that the general characteristics of disturbance waves in the developed region are:

(a) After a short distance $L/D = 30$ the waves attain a constant speed which is proportional to the gas velocity and only weakly dependent on the liquid flow.
(b) The separations between the waves converge towards a constant which is independent of both liquid flow and gas velocity.

We now turn to the evidence concerning the profile of the waves.

2.3. Transport in the disturbance waves and sub-layer

It is not straightforward to find reliable data for the wave shape, largely because most experiments have been designed to study other features of annular flow. However, the data we present here suggest that it will be useful to divide the total film flow into the flow in the disturbance waves, and a 'sub-layer' of constant thickness. This will enable us to identify the extent to which liquid transport is dominated by the disturbance waves. Since the tube diameter greatly exceeds the film thickness, we adopt a two-dimensional model in which the film thickness h is partitioned as follows,

$$h = h_s + H;$$ (1)

here H is the wave thickness, and h_s is an average minimum thickness, to be defined in more detail in the following subsection. If the flow rate conveyed by the sub-layer is q_s, and the waves move with speed V and have an average wave height H_m, then, anticipating that there is small net flow through the wave, the total liquid flow rate is similarly partitioned as

$$q_l = VH_m + q_s.$$ (2)

The relative importance of these terms can be assessed using measurements of wave speed and height. Hazuku et al. (2008) obtained measurements of interfacial wave profiles and sub-layer thicknesses in an 11 mm tube at a distance $250D$ from the inlet using a laser focussed displacement meter (LFD), for two gas velocities and four liquid flow rates. Fig. 5(a) shows these results plotted in the form VH_m against q_{l0}.

Similar results were obtained by de Jong and Gabriel (2003) in a 9.525 mm tube at a distance $110D$ from the inlet using a parallel wire conductance technique, for gas velocities between 10 and 20 m/s and liquid flows between 100 and 700 mm²/s. Fig. 5b shows these results.

Both sets of data suggest that almost all the liquid flow is conveyed by the disturbance waves, the flow rate in the sublayer, q_s, being negligible in comparison with the net flow in the waves. Since the vast majority of the liquid flow occurs in the waves, the existence of the sub-layer may be considered irrelevant to the mathematical model in the following section.

We remark that a similar separation between sub-layer and waves was employed by Miya et al. (1971), in their study of what they termed 'roll waves'. In that case the gas velocity was lower and the sub-layer carried a more substantial fraction of the total liquid flow, but nonetheless the profile of the roll waves were quite similar to those of our disturbance waves.

2.4. Surface profiles

The paper of Wang et al. (2004) displays a film-thickness/time trace for flows of $U_g = 24.3$ m/s and q_{l0} of 285 m²/s in a 9.525 mm diameter tube (Fig. 3 in that paper). We have reproduced this trace as a spatial profile in Fig. 6, assuming a steady travelling wave velocity to convert the time domain to the space domain. The wave velocity is not quoted by Wang et al., but a value of 2.1 m/s is used since this is consistent with other measurements by de Jong and Gabriel (2003) for a similar tube and at similar flow rates. In Fig. 6 we have drawn the trace in terms of wave height H, subtracting the average of the minima between wave crests for the sublayer thickness h_s.

Wave profiles are also displayed in the paper of Zhao et al. (2013). Their Fig. 9 shows how the wavy surface evolves into a series of disturbance waves, which progressively aggregate to form a more well-defined sequence by $L/D = 58$. As mentioned earlier, they also show their disturbance waves becoming circumferentially coherent after a distance of about $20D$. Figure 14 of Zhao et al. shows time traces taken at four circumferential positions at $L/D = 58$ and at $U_g = 40$ m/s and $q_{l0} = 300$ mm²/s. In Fig. 7 we reproduce the trace for the probe at the 0° position, assuming a wave velocity of 4.1 m/s, which is predicted from the data of Wolf et al. (2001).

We emphasise that the axes in Figs. 6 and 7 are not to scale. From the point of view of the modelling, the most important property of the waves, apart from their uniform velocity and spacing, is that they have extremely small aspect ratio, of order 10^{-2}. We also note that the wave train in Fig. 6 suggests that the slope of the lee-ward face changes more abruptly than the slope of the upwind face.

3. A mathematical model

3.1. Setup

We now construct a mathematical model for disturbance waves that are sufficiently far downstream to have reached a steady profile. The waves are spatially periodic, with spacing S, and move with constant speed V. It is convenient to work in a frame moving with this speed V with respect to the fixed laboratory frame, as in Fig. 1. The initial liquid flow rate per unit of the tube perimeter is
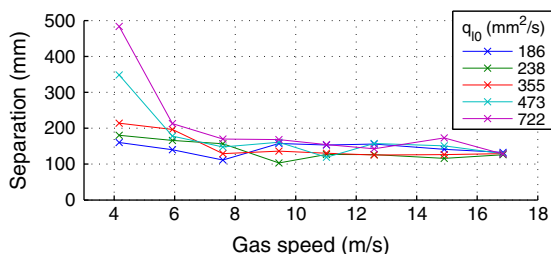

Fig. 4. Separation against gas speed for different initial liquid flow rates in a 9.5 mm tube. Data from de Jong and Gabriel (2003).
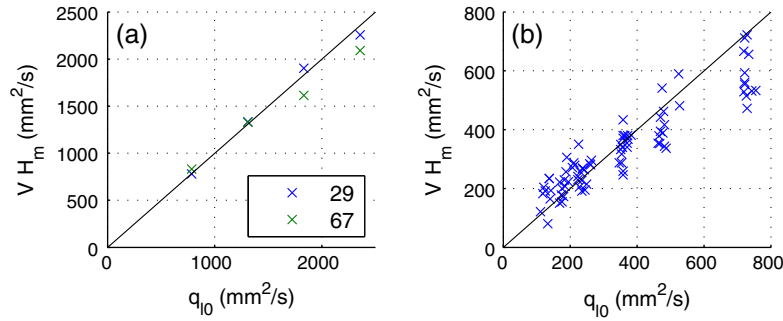
Fig. 5. Liquid flow rate in disturbance waves VH_m against initial liquid flow rate q_{l0}. Data from (a) Hazuku et al. (2008) and (b) de Jong and Gabriel (2003). In (a) the different colours refer to different gas flow rates.
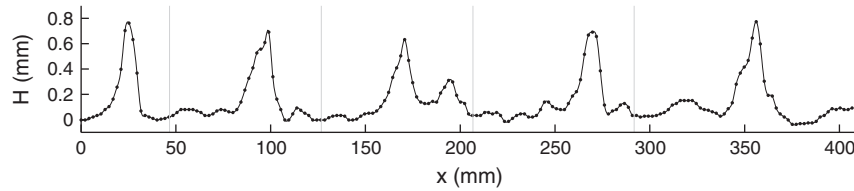

Fig. 6. Spatial wave profile showing film thickness above sub-layer. The waves are moving to the right. Vertical lines mark the boundaries between waves used for calculations in Section 4. Inferred from Wang et al. (2004).
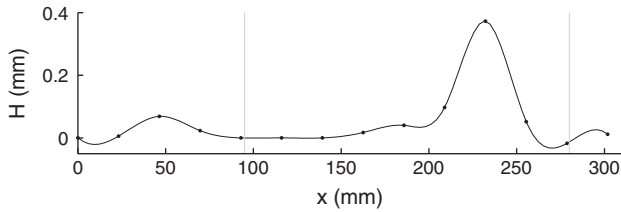

Fig. 7. Spatial wave profile showing film thickness above sub layer. Inferred from Zhao et al. (2013).

Fig. 8. Schematic illustration of a single disturbance wave in the moving frame. Panel (b) is the mathematical idealisation of (a), ignoring sub-layer. Region I is irrotational gas, region II is constant vorticity liquid, region III is constant vorticity gas.

q_{l0}, and we ignore any entrainment, so $q_l = q_{l0}$ is the liquid flux that is transported in the waves and underlying sub-layer.

From the discussion in Section 2.3, we neglect liquid flow within the sub-layer, and take $y = H(x)$ to be the height of the liquid interface above the sub-layer, y being the distance from the top of the sub-layer and x being the axial coordinate in the moving frame. The total liquid flow rate transported by the waves is then

$$q_l = \frac{V}{S} \int_0^S H(x)\,dx. \tag{3}$$

For a prescribed q_l, this expression can be used to determine the wave speed V once $H(x)$ and S are known. As remarked in connection with Fig. 3(a), it is an experimental observation that the waves move much slower than the gas, so the average gas speed in the moving frame is essentially the same as the prescribed gas flow rate, U_g.

Before we write down a model for this configuration, we recall that several high Reynolds number two-phase flows in the literature share the characteristic geometry of interfaces with small slope, and thin regions that have closed streamlines in the moving frame. For example Childress (1965) and O'Malley et al. (1991) have analysed flow past a backward facing step, and Fitt and Latimer (2000) and Riley (1987) have considered flow past sails and smooth indentations, respectively.

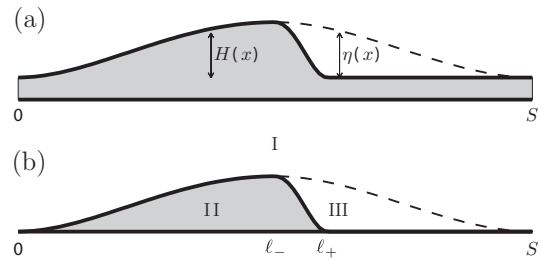The commonly accepted strategy is to assume that when such flows have attained steady state, the cumulative action of viscous forces at the interface is such that vorticity within the regions of closed streamlines is constant; this is in accordance with the Prandtl-Batchelor theorem (Batchelor, 1956). This, when coupled with the slenderness assumption, allows the dynamics of these regions to be described simply enough for 'effective' boundary conditions to be deduced for the perturbation they cause to the outer gas flow, which is nearly uniform. When physically acceptable smoothness conditions are applied at the extremities of the constant vorticity regions, nonlinear singular integral equations can be written down for the interface between the gas and liquid phases. This is the procedure we adopt below.[1]

3.2. Dimensional model

A single wave in the moving frame is shown in Fig. 8(a). The waves, which are separated by a distance S, are assumed only to have appreciable depth over the region $0 < x < \ell_+$. As remarked in Section 2.3, the diameter of the tube is large enough that the problem can be considered in a two-dimensional (S-periodic) half space $y > 0$ with far field gas flow at speed U_g.

---

[1] We remark that our early attempts to model the vorticity in a disturbance wave by one or more discrete vortices in the wave led to unrealistic wave profiles.

Following the discussion above, our model for the developed waves is as isolated regions of unknown constant vorticity liquid, behind which the gas separates to produces a recirculating wake, which also has constant vorticity. As remarked earlier, the leeward faces are steeper than the upwind faces, as in Fig. 8(b), in which the extraneous sub-layer has been omitted.

3.2.1. Gas region I (potential flow)

Assuming the gas is irrotational, the flow in region I is a potential flow, and we write the velocity there as $(u_g, v_g) = (U_g, 0) + \nabla\phi$. We have

$$\nabla^2\phi = 0 \qquad H(x) < y, \tag{4}$$

$$\phi_y = (U_g + \phi_x)H' \quad \text{on} \quad y = H(x), \quad \phi \to 0 \quad \text{as} \quad y \to \infty, \tag{5}$$

whilst Bernoulli's equation on the streamline $y = H(x)$ is

$$p_g + \frac{1}{2}\rho_g(U_g + \phi_x)^2 + \frac{1}{2}\rho_g\phi_y^2 = \frac{1}{2}\rho_g U_g^2 \quad \text{on} \quad y = H(x), \tag{6}$$

where ρ_g is the gas density, p_g is the gas pressure, and the choice of constant on the right-hand side corresponds to zero stagnation pressure.

3.2.2. Liquid region II (constant vorticity)

In region II, the liquid is assumed to have constant vorticity ω, and the liquid velocity is described by a stream function ψ, such that $(u_l, v_l) = (\psi_y, -\psi_x)$. We have

$$\nabla^2\psi = -\omega \qquad 0 < y < H(x), \quad 0 < x < \ell_+, \tag{7}$$

$$\psi = 0 \quad \text{on} \quad y = 0 \quad \text{and} \quad y = H(x), \quad 0 < x < \ell_+, \tag{8}$$

with Bernoulli's equation on the streamline $y = H(x)$ giving

$$p_l + \frac{1}{2}\rho_l|\nabla\psi|^2 = P \quad \text{on} \quad y = H(x), \quad 0 < x < \ell_+, \tag{9}$$

for liquid density ρ_l, liquid pressure p_l, and some unknown constant P.

3.2.3. Gas region III (constant vorticity)

In the wake region III, the gas is also assumed to have an unknown constant vorticity $\tilde{\omega}$, and its velocity is described by the stream function $\tilde{\psi}$, such that $(u_g, v_g) = (\tilde{\psi}_y, -\tilde{\psi}_x)$. We have

$$\nabla^2\tilde{\psi} = -\tilde{\omega} \qquad H(x) < y < \eta(x), \quad \ell_- < x < S, \tag{10}$$

$$\tilde{\psi} = 0 \quad \text{on} \quad y = H(x) \quad \text{and} \quad y = \eta(x), \quad \ell_- < x < S, \tag{11}$$

with Bernoulli's equation on the streamline $y = \eta(x)$ giving

$$\tilde{p}_g + \frac{1}{2}\rho_g|\nabla\tilde{\psi}|^2 = \tilde{P} \quad \text{on} \quad y = \eta(x), \quad \ell_- < x < S, \tag{12}$$

where $\tilde{p}_g$ is the gas pressure in this region, and $\tilde{P}$ is also an unknown constant.

3.2.4. Interface conditions

The pressure is continuous at the interfaces $y = H(x)$ and $y = \eta(x)$, so

$$p_g|_{y=H} = p_l|_{y=H} \qquad 0 < x < \ell_-, \tag{13}$$

$$p_g|_{y=\eta} = \tilde{p}_g|_{y=\eta} \qquad \ell_- < x < S. \tag{14}$$

We also require continuity of pressure across the liquid–gas interface in the leeward region,

$$p_l|_{y=H} = \tilde{p}_g|_{y=H} \qquad \ell_- < x < \ell_+. \tag{15}$$

As we shall see below, in the small aspect ratio limit it becomes impossible to satisfy this condition with $\ell_- \neq \ell_+$, and we will later impose pressure continuity between regions II and III directly at $\ell = \ell_- = \ell_+$, as in Fig. 9. For now however, we proceed with (15).

Finally, we also assume that neglected viscous effects ensure smooth attachment and reattachment of the streamlines, so

$$H(0) = H'(0) = 0, \qquad \eta(S) = \eta'(S) = 0, \tag{16}$$

$$H(\ell_-) = \eta(\ell_-), \qquad H'(\ell_-) = \eta'(\ell_-). \tag{17}$$

3.3. Dimensionless model

By observations such as those in Figs. 6 and 7, the liquid thickness H is small compared to the spacing and the length of the waves. Hence, we scale x and y with the separation S, H and η with the wave height H_0, and define the small parameters

$$\varepsilon = \frac{H_0}{S}, \qquad \rho = \frac{\rho_g}{\rho_l}. \tag{18}$$

The velocity perturbation in the gas will be of order εU_g, and the liquid velocity will therefore be of order $\varepsilon^{1/2}\rho^{1/2}U_g$, so as in O'Malley et al. (1991) or (Riley, 1987) we scale

$$\phi \sim \varepsilon U_g S, \qquad p_g, p_l, \tilde{p}_g, P, \tilde{P} \sim \varepsilon\rho_g U_g^2, \tag{19}$$

$$\psi \sim \rho^{1/2}\varepsilon^{1/2}U_g H_0, \qquad \tilde{\psi} \sim \varepsilon^{1/2}U_g H_0, \tag{20}$$

$$\omega \sim \rho^{1/2}\varepsilon^{1/2}\frac{U_g}{H_0}, \qquad \tilde{\omega} \sim \varepsilon^{1/2}\frac{U_g}{H_0}. \tag{21}$$

The linearised problem for the gas in region I (taking $\varepsilon \ll 1$) is then

$$\nabla^2\phi = 0 \qquad y > 0, \quad 0 < x < 1, \tag{22}$$

$$\phi_y = H' \quad \text{on} \quad y = 0, \qquad \phi \to 0 \quad \text{as} \quad y \to \infty, \tag{23}$$

$$p_g + \phi_x = 0 \quad \text{on} \quad y = 0. \tag{24}$$

Within the liquid and the wake it is convenient to write $y = \varepsilon Y$, and the leading order problem in region II, $0 < x < \ell_-$, is then

$$\psi_{YY} = -\omega \qquad 0 < Y < H(x), \tag{25}$$

$$\psi = 0 \quad \text{on} \quad Y = 0 \quad \text{and} \quad Y = H(x), \tag{26}$$

$$p_l + \frac{1}{2}\psi_Y^2 = P \quad \text{on} \quad Y = H(x), \tag{27}$$

and the problem in region III, $\ell_- < x < 1$, is

$$\tilde{\psi}_{YY} = -\tilde{\omega} \qquad H(x) < Y < \eta(x), \tag{28}$$

$$\tilde{\psi} = 0 \quad \text{on} \quad Y = H(x) \quad \text{and} \quad Y = \eta(x), \tag{29}$$

$$\tilde{p}_g + \frac{1}{2}\tilde{\psi}_Y^2 = \tilde{P} \quad \text{on} \quad Y = H(x). \tag{30}$$

The pressure continuity conditions at the interfaces are

$$p_g\big|_{y=0} = \begin{cases} p_l\big|_{Y=H} & 0 < x < \ell_-, \\ \tilde{p}_g\big|_{Y=\eta} & \ell_- < x < 1, \end{cases} \tag{31}$$

$$p_l\big|_{Y=H} = \tilde{p}_g\big|_{Y=H} \qquad \ell_- < x < \ell_+. \tag{32}$$

The boundary conditions for smooth detachment and reattachment at the ends of the wave are

$$H(0) = H'(0) = 0, \qquad \eta(1) = \eta'(1) = 0, \tag{33}$$

$$H(\ell_-) = \eta(\ell_-), \qquad H'(\ell_-) = \eta'(\ell_-). \tag{34}$$

Finally, the whole solution should be periodic with period 1, and the maximum of H should also be 1 (by the choice of scaling).

We must solve for the potential ϕ, the stream functions ψ and $\tilde{\psi}$, and the interface position $H(x)$. The unknown parameters, as yet, are $\omega, \tilde{\omega}, P, \tilde{P}, \ell_-$ and ℓ_+, which are to be determined as part of the solution. Although we will be able to argue that there is a unique *dimensionless* solution, we must remember that the separation length S and the wave height H_0 used in the non-dimensionalization are also unknown. Such lack of uniqueness

must be anticipated for a purely inviscid theory, and we shall see that it results in there being a two-parameter family of solutions.

Once $H(x)$ has been found, the dimensionless average wave height is

$$\sigma = \int_0^{\ell_+} H(x)\,dx, \tag{35}$$

and the liquid flux condition (3) then determines the *dimensional* wave speed as

$$V = \frac{q_l}{\sigma H_0}. \tag{36}$$

3.4. Impossibility of a shallow leeward face

The solution to the liquid problem (25)–(27) in region I is rather trivially

$$\psi = \frac{1}{2}\omega Y(H - Y), \quad \Rightarrow \quad p_l|_{Y=H} = P - \frac{1}{8}\omega^2 H^2, \tag{37}$$

while the problem (28)–(30) in region III has solution

$$\tilde{\psi} = \frac{1}{2}\tilde{\omega}(\eta - Y)(Y - H),$$
$$\Rightarrow \quad \tilde{p}_g|_{Y=\eta} = \tilde{p}_g|_{Y=H} = \tilde{P} - \frac{1}{8}\tilde{\omega}^2(\eta - H)^2, \tag{38}$$

The pressure condition (32) on the liquid–gas interface in $\ell_- < x < \ell_+$ therefore requires

$$\tilde{P} - \frac{1}{8}\tilde{\omega}^2(\eta - H)^2 = P - \frac{1}{8}\omega^2 H^2. \tag{39}$$

From $x = \ell_-$ where $H = \eta$, this determines $P = \tilde{P} + \frac{1}{8}\omega^2\eta(\ell_-)^2$, and so for $x = \ell_+$ where $H = 0$ it would require

$$-\frac{1}{8}\tilde{\omega}^2\eta(\ell_+)^2 = \frac{1}{8}\omega^2\eta(\ell_-)^2. \tag{40}$$

This is evidently not possible (except in the uninteresting case $\omega = \tilde{\omega} = 0$). We are thus led to the conclusion that it is impossible to have the constant vorticity liquid region and the constant vorticity wake region overlapping – at least in the shallow aspect ratio approximation. The interface must be steep enough to be treated instead as the abrupt transition in Fig. 9, at $x = \ell$, and we impose

$$p_l = \tilde{p}_g \quad \text{at} \quad x = \ell, \tag{41}$$

Having steepened the leeward face in this manner, it is then convenient to reduce the notation by redefining $H(x)$ as both the liquid–gas interface (in $x < \ell$) and the separating gas streamline (in $x > \ell$),

$$H(x) = \begin{cases} H(x) & 0 < x \leqslant \ell, \\ \eta(x) & \ell < x < 1. \end{cases} \tag{42}$$

3.5. Reduction to an integral equation

The gas problem (22)–(24) has solution given by the periodic Hilbert transform (*e.g.* Carrier et al., 1966)

$$p_g|_{y=0} = -\int_0^1 H'(\xi)\cot\pi(x - \xi)\,d\xi, \tag{43}$$
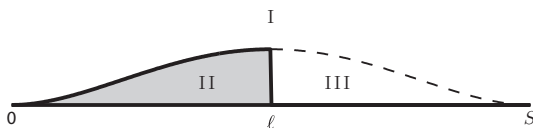

Fig. 9. Schematic of the model wave in the limit $\ell_- = \ell_+ = \ell$.

and the pressure condition (31) requires this to balance the pressure in the liquid and the wake. The liquid pressure was given earlier in (37), and with the modified notation the wake problem (28)–(30) has solution

$$\tilde{\psi} = \frac{1}{2}\tilde{\omega}Y(H - Y), \quad \Rightarrow \quad \tilde{p}_g|_{Y=H} = \tilde{P} - \frac{1}{8}\tilde{\omega}^2 H^2, \tag{44}$$

on $\ell < x < 1$. Combining, we see that the interface therefore satisfies a Fredholm integral equation of the second kind, namely

$$\int_0^1 H'(\xi)\cot\pi(x - \xi)\,d\xi = \begin{cases} -P + \frac{1}{8}\omega^2 H^2 & 0 < x < \ell, \\ -\tilde{P} + \frac{1}{8}\tilde{\omega}^2 H^2 & \ell < x < 1, \end{cases} \tag{45}$$

with conditions

$$H(0) = H'(0) = H(1) = H'(1) = 0, \tag{46}$$

and with

$$P - \frac{1}{8}\omega^2 H(\ell)^2 = \tilde{P} - \frac{1}{8}\tilde{\omega}^2 H(\ell)^2. \tag{47}$$

3.6. Solution of the integral equation

We now make the key observation that, if $\tilde{\omega} = \omega$, then from (47) $\tilde{P} = P$, and the problem in (45) is identical over the two intervals. It is therefore equivalent to a train of isolated liquid packets with constant vorticity interacting with an unseparated potential flow, the interface $H(x)$ satisfying

$$\int_0^1 H'(\xi)\cot\pi(x - \xi)\,d\xi = -P + \frac{1}{8}\omega^2 H^2,$$
$$H(0) = 0, \quad H'(0) = 0, \quad \max_{0 < x < 1} H = 1. \tag{48}$$

Although it is not immediately clear that this is the only possible situation in which the integral Eq. (45) has a solution, we have been unable to find convergent numerical solutions with $\tilde{\omega} \neq \omega$. We remark that although the dimensionless vorticities are the same in the liquid and wake regions for this solution, the physical vorticity is not the same because they have been scaled differently.

Somewhat intriguingly, the problem with $\tilde{\omega} = \omega$ in (48) is then independent of ℓ. Having thus determined the profile $H(x)$ for the combined wave height and separating streamline, we can seemingly choose any location we like for the separation point ℓ and the steep leeward face of the wave. It is apparent that the solution for $H(x)$ is symmetric, giving rise to a pressure minimum at the midpoint. We therefore argue on physical grounds that this is the most reasonable location for the separation of the gas wake from the film, so that $\ell = \frac{1}{2}$ and $H(\frac{1}{2}) = 1$.

The problem (48), with symmetry about $x = \frac{1}{2}$, has been solved numerically using the method of Forbes (1985), and the solution is shown in Fig. 10. Unique values of P and ω are determined, and we denote the latter as $\omega_* \approx 7.62$ for use below.

Briefly, the numerical method consists of discretizing the interface on a uniform grid $x_i = i/N, i = 0, \ldots N$, and solving (48) as a nonlinear algebraic system for the values H_i, P, and ω. The integral transform is calculated using a simple trapezium rule with the derivatives $H'(\xi)$ and the transform kernel $\cot\pi(x - \xi)$ evaluated at midpoints $\xi_j = \frac{1}{2}(x_j + x_{j+1})$; this symmetric discretization is sufficient to negotiate the singularity of the kernel at $\xi = x$. Values of $H_0 = H_N = 0$ are imposed at the end points, and the integral equation is satisfied at each of the $N - 1$ interior points. The additional constraints $H = 1$ at the mid point, and $H'(x) = 0$ at $x = 0$ effectively serve to determine P and ω.

The key result to follow from this solution is given by the flux condition (36), which determines the wave speed as
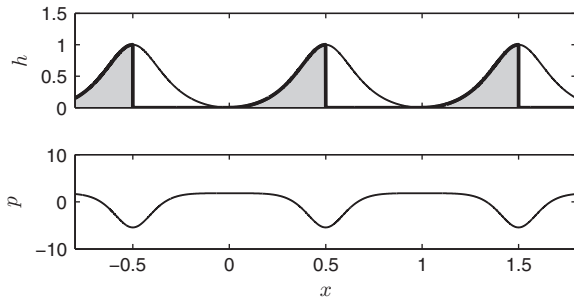
Fig. 10. Numerical solution of (48) for $H(x)$ with $H(\frac{1}{2}) = 1$, and with the interface between liquid and wake taken to lie where the pressure gradient changes sign at $\ell = \frac{1}{2}$. The lower panel shows the corresponding pressure from (43). The corresponding Bernoulli constant is $P_* \approx 1.81$, and the vorticity is $\omega_* \approx 7.62$.

$$V = \frac{q_l}{\sigma H_0}, \tag{49}$$

where σ is the area beneath half of the profile,

$$\sigma \equiv \int_0^{1/2} H(x)\,\mathrm{d}x \approx 0.183. \tag{50}$$

We remark that this does not unfortunately provide a *prediction* of the wave velocity, due to the non-uniqueness of the wave height H_0, which must be determined by some additional physics but which is likely to depend on both of the gas and liquid flow rates. The missing physics concerns the detailed role of viscosity in establishing the constant vorticity regions; similar non-uniqueness questions arose in Riley (1987).

Similarly, the unique value found for the dimensionless vorticity does not mean we have determined the actual physical vorticity, since that also depends on the undetermined separation and height. However, redimensionalizing that value, we predict a relationship between the dimensional vorticity, wave separation S and wave height H_0, namely

$$\rho_l H_0 S \omega^2 = \omega_*^2 \rho_g U_g^2. \tag{51}$$

4. Discussion

Our mathematical model suggests that there is a two-parameter family of solutions for the waves. The most natural parameters to take are the spacing S and the height H_0, and the fundamental results to follow from the analysis are the wave area and liquid flux transported by the wave,

$$A = SH_m = \sigma SH_0, \qquad q_l = VH_m = \sigma VH_0, \tag{52}$$

where the model predicts $\sigma \approx 0.183$. It is possible to use certain specific pieces of data to indicate support for this shape factor, either from

$$\sigma = \frac{H_m}{H_0}, \tag{53}$$

or from

$$\sigma = \frac{A}{H_0 S}. \tag{54}$$

We apply these estimates for the five wave crests seen in the experimental data in Fig. 6. The value used for substrate thickness h_s is an average of the minimum values, in this case 0.32 mm. The results are summarised in Table 1.

These σ values are derived from a very small sample but they do indicate a value not far from the theoretical model prediction of 0.183. However it should also be noted that the traces show the

Table 1
Estimates of σ inferred from the data of Wang et al. (2004). Average and maximum wave heights are taken directly from that paper, and the area and separation are found by integrating the trace shown in Fig. 6.

Wave	H_0 (mm)	H_m (mm)	A (mm^2)	S (mm)	σ (53)	σ (54)
1	0.774	0.129	19.26	127.7	0.166	0.195
2	0.692	0.169	18.46	140.4	0.244	0.190
3	0.633	0.153	18.93	118.1	0.214	0.253
4	0.692	0.153	16.63	108.5	0.221	0.222
5	0.762	0.157	12.59	83.0	0.206	0.199
Mean					0.210	0.201

presence of intermediate ripples with heights considerably less than the heights of the main waves. From the reported frequency data it is apparent that these are also counted as disturbance waves and they are included in any evaluation of average interface height or area under the wave. Of course, such waves are not considered in our theoretical model.

Values of σ can also be inferred from the paper by Zhao et al. (2013), from which Fig. 7 is taken. Their Fig. 14 shows time traces taken at four circumferential positions at a distance of $58D$ and at $U_g = 40$ m/s and $q_{l0} = 300$ mm^2. Eight large waves are shown but again there are a number of intermediate ripples. Table 2 shows the numbers, which are the average value for the eight larger waves. This time the σ value is less than the model value but again is only one result from a small sample. The particular wave shape in Fig. 7, shows the same general shape as the model. The area under the graph between the two marked limits is 13.5 mm^2, $S = 163$ mm and $H_0 = 0.386$. Hence the σ value for that particular wave is 0.215.

Our prediction of σ is also in accordance with estimates of around 5 for the ratio of maximum wave height to mean thickness reported by Hewitt and Nicholls (1969).

The second main conclusion of the model is the relationship (51) between wave separation, height, and vorticity,

$$\rho_l H_0 S \omega^2 \approx 58 \rho_g U_g^2. \tag{55}$$

We can use experimental data for H_0, S and U_g to calculate the vorticity from this relationship for different conditions. The result is hard to test, however, since we have no clear method of explicitly determining the vorticity from available data. A validation of this relationship must await future development of measurement techniques and detailed experiments.

Nevertheless, it is important to investigate whether the key features of disturbance waves identified in Section 2 are in fact consistent with this relationship. We recall from Section 2.2 that (i) the wave separation S was seen to be almost independent of both gas speed and liquid flow rate, and (ii) the wave speed V was found to increase roughly linearly with gas speed but largely independent of liquid flow. Although it is not possible to predict these observations because of the non-uniqueness of the solution of our dimensional model, we can see from the result in (49) that this behaviour for V would require H_0 to vary in proportion to q_l/U_g. Adopting such a dependence in (55) and remembering that S is nearly

Table 2
Estimates of σ inferred from the data of Zhao et al. (2013).

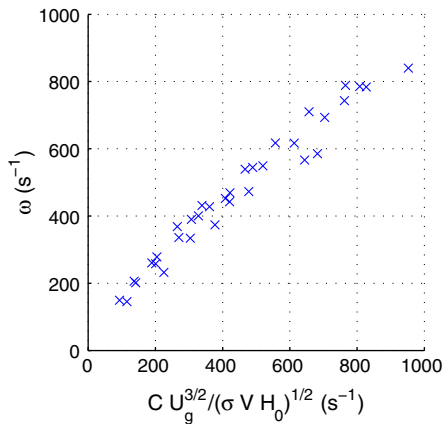| Position	270°	180°	90°	0°	Mean
h_0 (mm)	0.360	0.395	0.404	0.387	0.386
h_m (mm)	0.123	0.131	0.130	0.126	0.128
h_s (mm)	0.087	0.092	0.092	0.092	0.091
H_m (mm)	0.036	0.039	0.038	0.034	0.037
H_0 (mm)	0.273	0.303	0.312	0.296	0.296
σ	0.133	0.128	0.123	0.116	0.125

Fig. 11. Wave vorticity ω plotted against $U_g^{3/2}/(\sigma V H_0)^{1/2}$ for the data of de Jong and Gabriel (2003), encompassing a range of different gas and liquid flow rates. Vorticity ω is calculated from (55) and $C \approx 0.13 \text{ m}^{-1/2}$ is a constant scaling factor.

independent of both U_g and q_l, our theory necessarily implies, when coupled with this observational evidence, that the vorticity varies with U_g and q_l according to

$$\omega = C \frac{U_g^{3/2}}{q_l^{1/2}}, \tag{56}$$

for some scaling constant C, with dimensions 1/length$^{1/2}$.

We have used the data of de Jong and Gabriel (2003) to test this relationship; some of their data were shown earlier in Fig. 4. We infer experimental measurements of H_0, S, and V, for varying gas speed and initial liquid flow rates. From those, we calculate ω using (55) and q_l using (52). Fig. 11 shows the results, and suggests that indeed the vorticity follows (56) quite closely; this in turn implies that

$$S = \alpha \frac{V}{U_g}, \tag{57}$$

for all V and U_g, where $\alpha = \sigma \omega_*^2 \rho_g / \rho_l C^2$. However, to go one step further and allow the model to truly *predict* this behaviour, a more detailed theory – or better still experimental evidence – will be needed to explain the dependence of the vorticity seen in (56). We emphasise that (56) has been neither derived nor refuted by the current model; it is simply the relationship that is anticipated to yield consistency with the observations. The fact that the experimental data in Fig. 11 agrees with this dependence nevertheless lends support to our theory.

5. Conclusion

We have presented a mathematical model which provides new insights into the most distinctive features of disturbance waves in two-phase pipe flow, in the regime in which inertial forces dominate. Over a wide range of inlet liquid and gas flow rates, these waves have heights H_0 and spacing S that are constant in a frame moving with the wave speed V, and our model predicts relations between these quantities and the inlet flows.

By exploiting the smallness of the aspect ratio of the waves, and using the Prandtl-Batchelor theorem, we have simplified the free-boundary problem for the liquid/gas interface into a single integral equation. In dimensional form, this equation contains just two of the parameters, V, H_0 as well as the vorticity in the disturbance waves ω. However, the model can be non-dimensionalised and solved numerically to give a unique disturbance wave profile, and this implies that the net liquid flow in the waves is $q_l \approx 0.183 V H_0$, which is in good agreement with experimental evidence.

The model is also consistent with the scenario that the disturbance waves transport the majority of the liquid flow, riding on a liquid sublayer in which there is negligible flow and whose thickness is essentially irrelevant. When our model predictions are combined with experimental information from de Jong and Gabriel (2003), the results suggest that the vorticity in the wave is proportional to $U_g^{3/2}/q_l^{1/2}$, as in Fig. 11. This in turn suggests that S is related linearly to V/U_g through the relationship in (57).

References

Batchelor, G.K., 1956. A proposal concerning laminar wakes behind bluff bodies at large Reynolds number. J. Fluid Mech. 1, 388–398.

Belt, R.J., Van't Westende, J., Prasser, H., Portela, L., 2010. Time and spatially resolved measurements of interfacial waves in vertical annular flow. Int. J. Multiphase Flow 36, 570–587.

Carrier, G., Krook, M., Pearson, C., 1966. Functions of a Complex Variable: Theory and Technique. McGraw-Hill, pp. 417.

Childress, S., 1965. Solutions of Euler's equations containing finite eddies. Phys. Fluids 9, 860.

de Jong, P., Gabriel, K.S., 2003. A preliminary study of two-phase annular flow at microgravity: experimental data of film thickness. Int. J. Multiphase Flow 29, 1203–1220.

Fitt, A., Latimer, T., 2000. On the unsteady motion of two-dimensional sails. IMA J. Appl. Math. 65, 147–171.

Forbes, L.K., 1985. On the effects of non-linearity in free-surface flow about a submerged point vortex. J. Eng. Math. 19, 139–155.

Hazuku, T., Takamasa, T., Matsumoto, Y., 2008. Experimental study on axial development of liquid film in vertical upward annular two-phase flow. Int. J. Multiphase Flow 34, 111–127.

Hewitt, G., Nicholls, B., 1969. Film thickness measurement in annular two-phase flow using a fluorescence spectrometer technique. Part II: Studies of the shape of disturbance waves, U.K.A.E.A. Research Group, Harwell, UK.

Hewitt, G., Hall Taylor, N., 1970. Annular Two-Phase Flow. Pegammon Press, UK.

Miya, M., Woodmansee, D., Hanratty, T., 1971. A model for roll waves in gas–liquid flow. Chem. Eng. Sci. 26, 1915–1931.

Nedderman, R., Shearer, C., 1963. The motion and frequency of large disturbance waves in annular two-phase flow of air–water mixtures. Chem. Eng. Sci. 18, 661–670.

O'Malley, K., Fitt, A., Jones, T., Ockendon, J., Wilmott, P., 1991. Models for high-Reynolds-number flow down a step. J. Fluid Mech. 222, 139–155.

Riley, N., 1987. Inviscid separated flows of finite extent. J. Eng. Math. 21, 349–361.

Schubring, D., Shedd, T., Hurlbert, E., 2010. Studying disturbance waves in vertical annular flow with high speed video. Int. J. Multiphase Flow 36, 825–835.

Schubring, D., Shedd, T., Hurlbert, E., 2010. Planar laser-induced fluorescence (PLIF) measurements of liquid film thickness in annular flow Pt I. Int. J. Multiphase Flow 36, 385–396.

Hall Taylor, N., Hewitt, G., Lacey, P., 1963. The motion and frequency of large disturbance waves in annular two-phase flow of air-water mixtures. Chem. Eng. Sci. 18, 537–552.

Wang, Z., Gabriel, K., Manz, D., 2004. The influences of wave height on the interfacial friction in annular gas–liquid flow under normal and microgravity conditions. Int. J. Multiphase Flow 30, 1193–1211.

Wolf, A., Jayanti, S., Hewitt, G., 2001. Flow development in vertical annular flow. Chem. Eng. Sci. 56, 3221–3235.

Zhao, Y., Markides, C., Hewitt, G., 2013. Disturbance wave development in two-phase gas–liquid upwards vertical annular flow. Int. J. Multiphase Flow 55, 111–129.